Biochimica et Biophysica Acta 1838 (2014) 1851–1861

Contents lists available at ScienceDirect

Biochimica et Biophysica Acta

journal homepage: www.elsevier.com/locate/bbamem

The effect of the chain length distribution of free fatty acids on the mixing properties of stratum corneum model membranes

Masashi Oguri [a,b], Gert S. Gooris [b], Kotatsu Bito [a], Joke A. Bouwstra [b,*]

[a] Analytical Science Research Laboratories, Kao Corporation, Akabane 2606, Ichikai, Haga, Tochigi 321-3497, Japan
[b] Leiden/Amsterdam Center for Drug Research, Department of Drug Delivery Technology, Leiden University, Einsteinweg 55, 2333 CC Leiden, the Netherlands

ARTICLE INFO

Article history:
Received 7 November 2013
Received in revised form 5 February 2014
Accepted 13 February 2014
Available online 22 February 2014

Keywords:
Stratum corneum
Skin
Lipid organization
Kinetics
FTIR

ABSTRACT

The stratum corneum (SC) plays a fundamental role in the barrier function of the skin. The SC consists of corneocytes embedded in a lipid matrix. The main lipid classes in the lipid matrix are ceramides (CERs), cholesterol (CHOL) and free fatty acids (FFAs). The aim of this study was to examine the effect of the chain length of FFAs on the thermotropic phase behavior and mixing properties of SC lipids. Fourier transform infrared spectroscopy and Raman imaging spectroscopy were used to study the mixing properties using either protonated or deuterated FFAs. We selected SC model lipid mixtures containing only a single CER, CHOL and either a single FFA or a mixture of FFAs mimicking the FFA SC composition. The single CER consists of a sphingoid base with 18 carbon atoms and an acyl chain with a chain length of 24 carbon atoms. When using lignoceric acid (24 carbon atoms) or a mixture of FFAs, the CER and FFAs participated in mixed crystals, but hydration of the mixtures induced a slight phase separation between CER and FFA. The mixed crystalline structures did not phase separate during storage even up to a time period of 3 months. When using palmitic acid (16 carbon atoms), a slight phase separation was observed between FFA and CER. This phase separation was clearly enhanced during hydration and storage. In conclusion, the thermotropic phase behavior and the mixing properties of the SC lipid mixtures were shown to strongly depend on the chain length and chain length distribution of FFAs, while hydration enhanced the phase separation.

1. Introduction

A primary function of the skin is to serve as a physical barrier in order to control the influences from the environment. This skin barrier is accomplished by the remarkably outermost layer of the skin; the stratum corneum (SC). It consists of dead cells (the corneocytes) embedded in a lipid matrix and the SC structure is often compared to a brick wall, in which the corneocytes are the bricks and the lipid matrix is the mortar [1]. The lipid matrix forms a continuous intercellular pathway in the SC which is considered to be an important route for the diffusion of substances across the SC [2]. The main lipid classes in the SC are ceramides (referred to as CERs), cholesterol (CHOL) and free fatty acids (referred to as FFAs) [3,4]. X-ray diffraction studies revealed that the lipids are organized in two coexisting lamellar phases with repeat distances of approximately 13 nm and 6 nm, referred to as the long periodicity phase (LPP) and the short periodicity phase (SPP), respectively [5]. At the human skin surface temperature, approximately 32 °C, the lipids within the lipid lamellae are organized mainly in an orthorhombic lateral packing, although a small population of lipids most probably also forms a hexagonal and/or a liquid lateral packing. The lamellar and lateral lipid organizations are considered to play an important role in the skin barrier function [6–8]. When focusing on the lipid composition, a wide distribution of FFA chain lengths are present in human SC. The most abundant chain lengths of the FFAs are 22, 24 and 26 carbon atoms, while FFAs with 16, 18 and 20 carbon atoms are less abundantly present [9]. As far as the CERs are concerned, twelve subclasses of CERs have been identified in human SC [10]. All CER subclasses are composed of a sphingoid base linked via an amide bond to a fatty acid. The various CER subclasses differ by the number of hydroxy groups in acyl chain and/or the number of OH groups and the presence of an unsaturated bonding. In addition in the SC each CER subclass shows a large distribution in chain lengths.

To understand the complex relationship among the skin barrier function, lipid organization and lipid composition, SC lipid mixtures have been studied. The composition of these models ranged from mixtures with a single CER, a single FFA and CHOL to mixtures comprising of complex multi-components of CERs, CHOL and FFAs [11–17]. Despite a large number of studies, little is known about the stability of these systems in time. Furthermore, it has been reported that the equimolar CERs/CHOL/FFAs mixtures form an orthorhombic lattice in which the CERs and FFAs participate in one lattice [11–13], while other papers report phase separation in other often less complex SC lipid model systems [14–17]. This may occur, either due to a difference in composition

* Corresponding author.
E-mail address: bouwstra@lacdr.leidenuniv.nl (J.A. Bouwstra).

http://dx.doi.org/10.1016/j.bbamem.2014.02.009
0005-2736/

of the mixtures and/or a difference in the preparation method. When focusing on the composition, CERs and FFAs have at least two factors which may affect phase separation, that is a variation in molecular architecture of the CERs and a variation in chain length distribution of CERs and FFAs.

The present study focuses on the thermotropic behavior and the mixing properties of the lipid mixtures during preparation and the physical stability of the lipid mixtures during hydration and storage. The lipid organization and the mixing behavior of the model mixtures were examined by Fourier transform infrared (FTIR) spectroscopy and Raman imaging spectroscopy. For the lipid composition a single CER with either a single FFA or a mixture of FFAs were selected. We chose the most abundant CER in the SC comprised of a non-hydroxy fatty acid (N) with a chain length of 24 carbon atoms linked to a sphingoid base (S) with 18 carbon atoms, referred to as CER NS [13,18]. For the FFAs either a chain length of 24C atoms (FFA24:0), 16C atoms (FFA16:0) or a complex mixture varying in chain length between FFA16:0 and FFA24:0 was used. This FFA mixture was also used in previous studies [13,18]. Our studies show that the mixing properties strongly depend on the chain length of the FFA and that hydration of the SC lipid mixtures enhances phase separation between FFA and CER NS.

2. Materials and methods

2.1. Chemicals

The synthetic CER NS(C24) was generously provided by Evonik (Essen, Germany). The CER classification system is according to Motta et al. [19]. The perdeuterated FFA (referred to as DFFA) with chain lengths of C18:0 and C20:0 were purchased from Cambridge Isotope Laboratories (Andover, Massachusetts). The DFFA with chain lengths of C16:0 and C22:0 were obtained from Larodan (Malmö, Sweden). The DFFA with a chain length of C24:0 was obtained from Arc Laboratories B.V. (Apeldoorn, The Netherlands). Cholesterol and acetate buffer salts were provided by Sigma-Aldrich Chemie GmbH (Schnelldorf, Germany). All organic solvents were manufactured by Labscan Ltd. (Dublin, Ireland). All chemicals used were of analytical grade.

2.2. Preparation of the lipid mixtures

Mixtures prepared in equimolar ratios of CER NS/CHOL/FFAs, CER NS/CHOL/FFA(C24) and CER NS/CHOL/FFA(C16) and their deuterated counterparts were prepared. The FFAs mixture consisted of fatty acids with chain lengths of C16:0, C18:0, C20:0, C22:0 and C24:0 in a molar ratio of 1.8%, 4.0%, 7.6%, 47.8% and 38.9%, respectively, mimicking the FFA composition in the SC [20].

2.3. Lipid mixtures for kinetic studies using FTIR

The preparation of lipid membranes on an AgBr window was performed as published elsewhere [13]. Briefly, lipids were dissolved in a mixture of chloroform/methanol and subsequently sprayed on the AgBr window using a Linomat IV (CAMAG, Muttenz, Switzerland). After spraying and drying, the lipid film was sandwiched between two AgBr windows and inserted in the FTIR device. Then the mixture underwent a thermal treatment as shown in Fig. 1. Shortly after spraying (P1 in Fig. 1) the sample was heated and subsequently equilibrated for 10 min at 90 °C. Then, the sample was cooled down to 20 °C (P2 in Fig. 1) and was kept for 10 min at this temperature. This heating/cooling cycle was repeated once more. The subsequent heating cycles were referred to as equilibration 1st (Eq1) and 2nd (Eq2). After the 2nd cycle and equilibration at 20 °C one of AgBr windows was removed and the sample was covered with 25 μl of a deuterated acetate buffer at pH 5 (50 mM). The deuterated buffer was used to avoid interference of the broad OH vibration peak with the CH_2 stretching vibrations in the FTIR spectrum. After hydration the sample was again sandwiched between AgBr windows and sealed with silicon glue to prevent dehydration. The sample was incubated for about 10 h at 37 °C and inserted in the FTIR device, after which the sample was cooled to 0 °C and subsequently heated to 90 °C. This heating process after hydration is referred to as Hyd. Then the sample was cooled to 20 °C. This point is referred to as After-Hyd (P6 in Fig. 1). During the heating and equilibration process FTIR spectra were monitored. Each spectrum was measured during 2 min. Subsequently, only the perdeuterated samples were stored at room temperature for 3 months to examine whether time-dependent changes occurred. The stored samples were measured by FTIR at regular time intervals at 20 °C (P7, P8 and P9 in Fig. 1).

2.4. FTIR measurements

All spectra were acquired on a Varian670 FTIR spectrometer (Varian Medical Systems, Inc.) equipped with a broad-band mercury cadmium telluride (MCT) detector. The sample was under continuous dry air purge for 30 min before data acquisition. The spectra were collected in transmission mode, as a coaddition of 134 scans (during Eq1 and Eq2) and 269 scans (during Hyd) at 1 cm^{-1} resolution. The lipid phase behavior during the equilibration process was examined between 20 °C and 90 °C during heating. The heating and cooling rates were 0.5 °C/min and 1.0 °C/min, respectively. After hydration at 37 °C, the sample was cooled to 0 °C, and was heated to 90 °C with a rate of 0.25 °C/min. Subsequently, the sample was cooled to 20 °C with a rate of 2.0 °C/min or 0.5 °C/min. The equilibration and hydration measurements were carried out with a time resolution of 120 s and 240 s, respectively. Time-dependent measurements were recorded with 128 scans at 1 cm^{-1} resolution at 20 °C. The software used was Varian

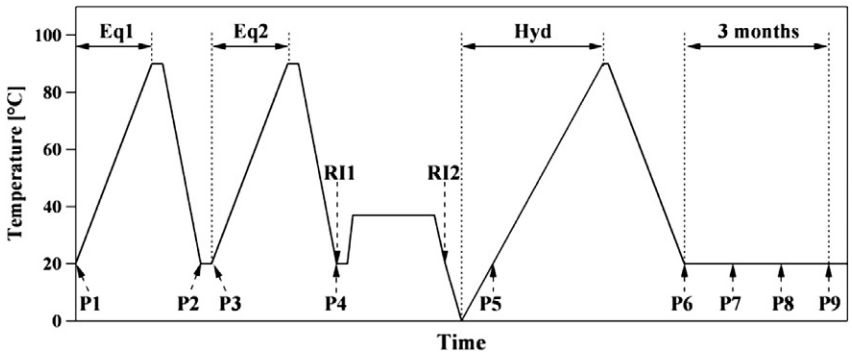

Fig. 1. Scheme of temperature controls and time dependence measurements including measurement points (P1 to P9).

Resolutions Pro. All the samples for investigating the thermal phase behavior were measured three times and the time-dependent changes were investigated at least twice.

2.5. Interpretation of FTIR spectrum

FTIR permits to monitor the conformational ordering and miscibility of the lipids within the crystalline packing [21,22]. In particular, the use of protonated and perdeuterated lipids allows simultaneous evaluation of the packing and miscibility properties of different classes of lipids in one lipid mixture. In this study we used perdeuterated free fatty acids. We focus on several vibrational modes providing information on the ordering and lateral packing of the hydrocarbon chains. The symmetric CH_2 stretching (2846–2855 cm^{-1}) and CD_2 stretching (2085–2100 cm^{-1}) modes provide information about the conformational order–disorder transitions (referred to as ν_sCH_2 and ν_sCD_2). Information on the packing of the carbon chains perpendicular to the chain direction is obtained from the CH_2 and CD_2 scissoring modes (referred to as δCH_2 (1462–1473 cm^{-1}) and δCD_2 (1085–1095 cm^{-1})). When the chains are in a crystalline orthorhombic lattice, the adjacent chains in scissoring and rocking modes interact via a short-range coupling, resulting in a broadening or splitting of the contours. The width of the splitting band is indicative of the domain size of the orthorhombic lattice [23]. However, when deuterated and protonated chains are mixed in one lattice, the chains will not interact and the vibrational coupling will not occur. Consequently, the splitting of the peak in the scissoring region of the spectrum will disappear [24]. Therefore, in an orthorhombic lattice, elimination of the coupling after replacing protonated lipids by deuterated ones is indicative of participation of the deuterated and protonated lipid classes in one lattice. In general, a phase transition temperature, for example the onset of the melting point, of a protonated chemical starts at a slightly higher temperature than that of the deuterated counterparts. In the FFA mixture used in this study this difference is 4 °C. However, as we deal mainly with FFA and CER that participate in the same lattice and we are focusing on mixing and not on the phase transition temperatures, the deuteration of FFA will not influence the outcome of our studies. Furthermore, it is a prerequisite to use the DFFA in order to investigate the mixing property between CER and FFA.

2.6. Determining the midpoint temperature of the phase transition in FTIR spectrum

In FTIR, the frequency of the ν_sCH_2 is indicative for the conformational ordering of the lipid chains: a higher wavenumber is indicative for an increased disordering. When plotting the maximum of the ν_sCH_2 vibration as a function of temperature, two lipid phase transitions can be detected in the lipid mixtures, the orthorhombic (OR)–hexagonal (HEX) phase transition and the hexagonal–liquid (LIQ) phase transition. The midpoint temperatures of the OR–HEX phase transition (T_{OR-HEX}) and HEX–LIQ phase transition ($T_{HEX-LIQ}$) were determined by fitting with five (two transitions) or three linear functions (single transition) to use a six-pair-parameter or a four-pair-parameter of the temperature and frequency, respectively. As one example, when fitting data of the ν_sCH_2 vibrations in Hyd of the protonated sample with five linear functions, the first and last parameters of the temperature were fixed at 0 °C and 90 °C, respectively. T_{OR-HEX} was defined by the midpoint between the temperatures of the second and third parameters, and the temperature width of the OR–HEX phase transition (TW_{OR-HEX}) was defined by the difference in the temperature of the second and third parameters. Similarly, $T_{HEX-LIQ}$ was defined as the midpoint between the temperatures of the fourth and fifth parameters, while the temperature width of the HEX–LIQ ($TW_{HEX-LIQ}$) was the difference in temperature of the fourth and fifth parameters.

2.7. Evaluation of the peak width of ν_sCH_2 and ν_sCD_2 modes in FTIR

To evaluate the peak width of the ν_sCH_2 mode, the ν_sCH_2 peak was base line-corrected between 2825 cm^{-1} and 2875 cm^{-1} and was normalized by the maximum intensity value. This data treatment was carried out without smoothing of the spectrum. Similarly, the ν_sCD_2 peak was base line-corrected between 2065 cm^{-1} and 2120 cm^{-1} and was normalized by the maximum intensity value.

2.8. Raman imaging spectroscopy

For Raman imaging spectroscopy, the equimolar CER NS/CHOL/DFFAs and CER NS/CHOL/DFFA(C16) were selected. The sample preparation was slightly different from that used for the FTIR measurements, but closely mimicked that corresponding to the RI1 (twice heating and cooling) and RI2 (an additional 10 min hydration at 37 °C) in Fig. 1. (1) A cover glass was used as a substrate for spraying the lipid mixtures. (2) The equilibration was carried out in an aluminum container on a heater. The heating to 90 °C and the cooling to room temperature took an approximately 40 min and 60 min, respectively. (3) The sample was hydrated overnight at a temperature of 20 °C. Each sample was prepared twice and measured with Raman spectroscopy.

2.9. Raman imaging measurements

We used a confocal Raman microspectrometer (Nanofinder ®30, Tokyo Instrument Inc.). The 632.8 nm line of a He–Ne laser (MellesGriot 05-LHP-928) was focused on a sample. At the sample position the laser power was approximately 8 mW. A 100× objective (Nikon, S Fluor) with a numerical aperture (NA) of 1.3 was used. The backward Raman scattering was collected by the same objective. After passing through a 100 μm pinhole, the scattered light was introduced into the spectrometer and detected by a CCD detector (Andor DU401A BR-DD). All the spectra were background subtracted and intensity-corrected. In the Raman mapping measurement, the excitation laser spot scanned a sample surface area of 30 μm × 30 μm. The laser spot was translated by galvano-mirrors horizontally with a 1 μm step in both x and y directions. Spatial resolution is less than 1 μm in the lateral direction. The exposure time for each spectrum was 1 s. In each sample two or three different areas were measured.

2.10. Visualization method of Raman spectroscopy

All spectral were processed (i.e., baseline correction and peak area calculations) with Igor Pro software (WaveMetrics). Three peaks, 700 cm^{-1} (ring breathing from CHOL), 1300 cm^{-1} (CH_2 twisting from CER NS) and 2100 cm^{-1} (CD_2 stretching from DFFA (DFFAs or DFFA(C16))), were used for Raman mapping. The peak area of CER was calculated after subtraction of linear baseline in the region of interest. Subsequently, the peak area was normalized by the maximum peak area of CER in all spectra. Peak areas of CHOL and DFFA were treated with the same method as that of CER.

3. Results

3.1. Thermal behavior of the stretching vibrations of SC lipid models

Fig. 2(A), (B) and (C) show the thermal behavior of the ν_sCH_2 vibrations of CER NS/CHOL/DFFAs during the various heating processes, that is Eq1, Eq2 and Hyd, respectively. The ν_sCH_2 vibrations at 20 °C of Eq1, Eq2 and Hyd are 2851.2 cm^{-1}, 2850.4 cm^{-1} and 2850.0 cm^{-1}, respectively. The ν_sCH_2 vibrations below 2850 cm^{-1} indicate highly ordered hydrocarbon chains. Upon heating, the ν_sCH_2 vibration shifts toward a higher wavenumber. Overall, two shifts can be identified. The first small shift, between 20 °C and 30 °C, suggests an OR–HEX phase change [13]. This small shift is not visible in the curve of the thermotropic

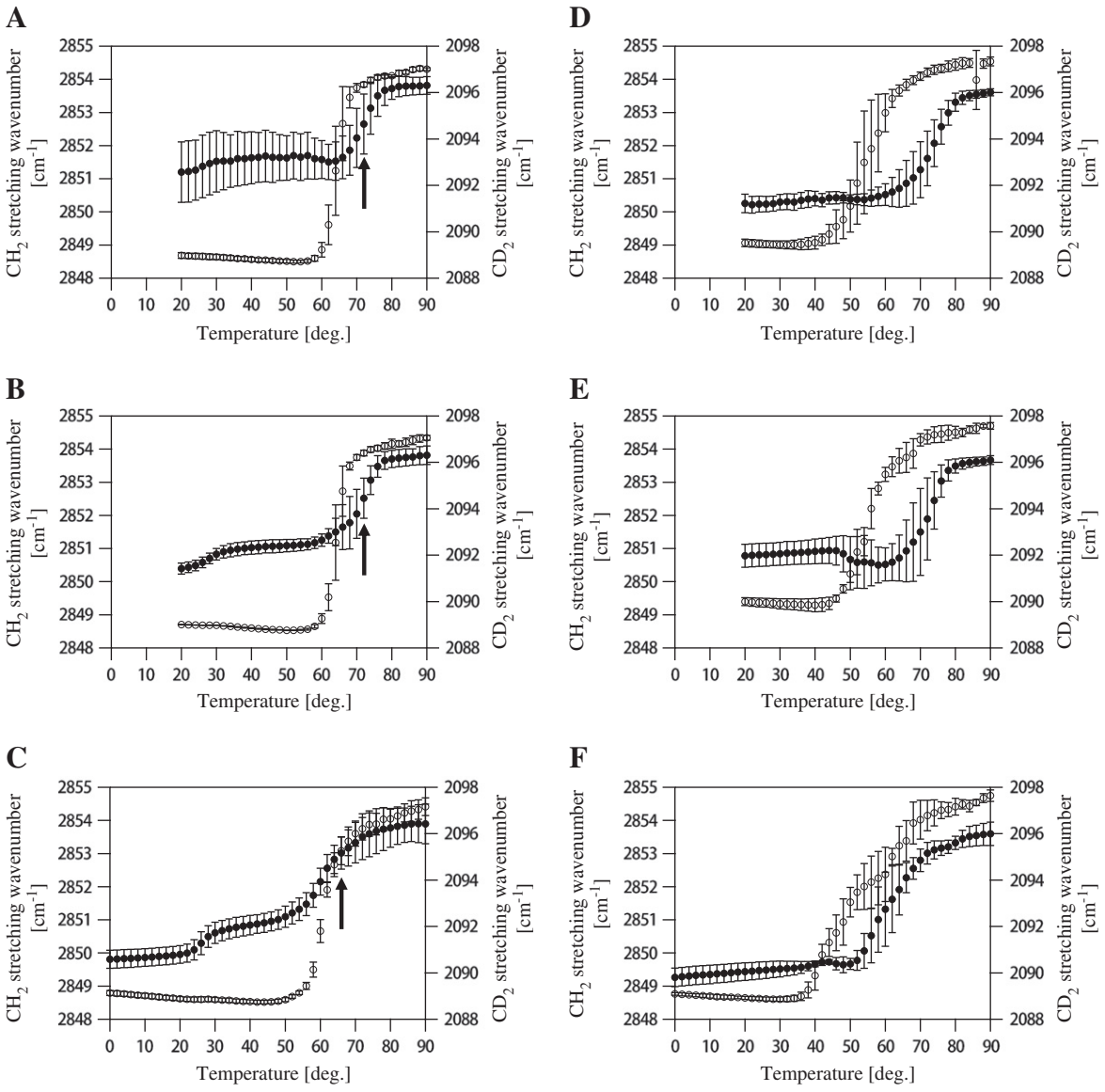

Fig. 2. Thermotropic response of the CER NS/CHOL/DFFAs and CER NS/CHOL/DFFA(C16) mixtures as probed with the $\nu_s CH_2$ and $\nu_s CD_2$ vibrations. (●) $\nu_s CH_2$ band position, (○) $\nu_s CD_2$ band position. (A) 1st equilibration, (B) 2nd equilibration and (C) hydration for the CER NS/CHOL/DFFAs. (D) 1st equilibration, (E) 2nd equilibration and (F) hydration for the CER NS/CHOL/DFFA(C16). Each data point represents the mean ± S.D. (standard deviation) of three experiments.

response in Fig. 2(A). The second strong shift is between 50 °C and 75 °C and is indicative for an order–disorder phase change [13]. These phase transitions have also been observed by wide-angle X-ray diffraction. However, in the previous study the transition temperatures are slightly different due to a difference in sample composition [25].

Simultaneously the vibrations of the DFFA are monitored in the infrared spectrum. Fig. 2(A), (B) and (C) depict the $\nu_s CD_2$ vibration as a function of temperature of CER NS/CHOL/DFFAs. Below 50 °C, the frequency of this vibration is lower than 2089 cm^{-1} in the three heating curves, suggesting that also acyl chains of the DFFA are highly ordered [14,26]. Upon heating, the $\nu_s CD_2$ vibration shifts gradually toward a higher wavenumber. A major shift appears between 50 °C and 70 °C, demonstrating an order–disorder phase change [13].

When comparing the order–disorder transition of the protonated and deuterated chains, this phase change occurs in almost the same temperature range. This suggests an associated phase change of the protonated and deuterated chains. Between 20 °C and 30 °C, small shifts of the $\nu_s CH_2$ vibrations are observed, while no changes in the $\nu_s CD_2$ vibrations are detected. It has been reported that the $\nu_s CD_2$ vibration is less sensitive for such an OR–HEX phase transition than the $\nu_s CH_2$ vibration [13].

When comparing the heating curves reflecting the different stages of the sample preparation process, the $\nu_s CH_2$ and $\nu_s CD_2$ vibrations demonstrate a very similar thermal behavior with three small differences. First, the order–disorder phase transition temperature of Hyd in the $\nu_s CH_2$ vibration shows a small shift to lower temperatures than those in the curves of Eq1 and Eq2. The temperature range in which this phase transition of hydrated lipids (Hyd) occurs is decreased by about 7 °C compared to that of dry lipid mixtures (Eq1 and Eq2), see arrows ($T_{HEX-LIQ}$) in Fig. 1. Second, the wavenumbers of the $\nu_s CH_2$ vibrations in the low temperature range decreases in the sequence Eq1, Eq2 and Hyd, while the $\nu_s CD_2$ vibrations are almost the same among the three samples. Third, minor but significant changes are observed in the width and wavenumber of the $\nu_s CH_2$ peak at temperatures below the OR–HEX phase transition, see Fig. 3(A). The $\nu_s CH_2$ spectrum of Eq1 shows a broader peak compared to those of Eq2 and Hyd and the peak-top wavenumber of Eq1 is slightly higher than those of Eq2 and Hyd. However, no significant difference is observed in the $\nu_s CD_2$ spectra at 20 °C when comparing Eq1, Eq2 and Hyd, see Fig. 3(B).

When replacing the DFFAs by the single fatty acids DFFA(C24) the thermal behavior of the $\nu_s CH_2$ vibration is similar to that of the CER NS/CHOL/DFFAs (data not shown).

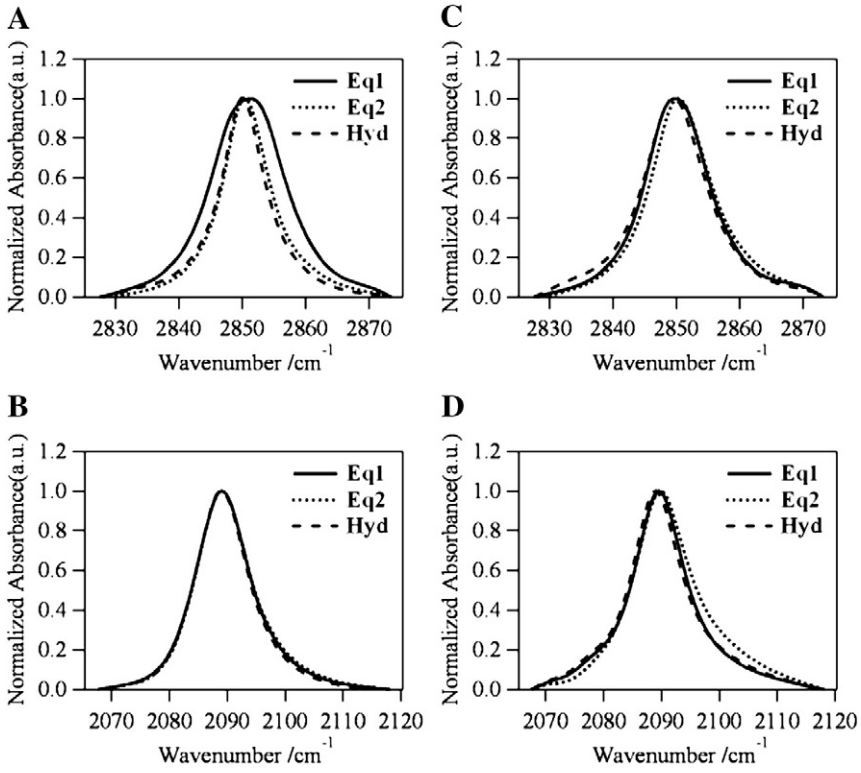

Fig. 3. Infrared spectra of the CER NS/CHOL/DFFAs and CER NS/CHOL/DFFA(C16) mixtures. (A) The spectra of the $\nu_s CH_2$ vibration and (B) the spectra of the $\nu_s CD_2$ vibration for the CER NS/CHOL/DFFAs. (C) The spectra of the $\nu_s CH_2$ vibration and (D) the spectra of the $\nu_s CD_2$ vibration for the CER NS/CHOL/DFFA(C16). All spectra are collected at 20 °C in Eq1 (solid line), Eq2 (dotted line) and Hyd (broken line).

Fig. 2(D), (E) and (F) show the thermal behavior of the $\nu_s CH_2$ and $\nu_s CD_2$ vibrations of CER NS/CHOL/DFFA(C16) of the three heating runs, which are clearly different from those of CER NS/CHOL/DFFAs and CER NS/CHOL/DFFA(C24). The $\nu_s CH_2$ and $\nu_s CD_2$ vibrations in Eq1 are characterized by only one shift between 60–80 °C (2850.3 to 2853.6 cm^{-1}) and 40–80 °C (2089.5 to 2097.2 cm^{-1}), respectively. This indicates different order–disorder temperature ranges of the $\nu_s CH_2$ and $\nu_s CD_2$ vibrations, and thus a less associated phase change of the protonated and deuterated chains. This means that the thermotropic behavior of DFFA(C16) and CER NS in this temperature range are different. A similar thermotropic behavior is observed in Eq2 and Hyd, see Fig. 2(E) and (F). However, there is also a difference among Eq1, Eq2 and Hyd. This concerns the slight temporary shift to lower $\nu_s CH_2$ wavenumber in the spectrum during Eq2 and Hyd in the temperature range 45–60 °C and 45–50 °C, respectively, which is not observed in the spectrum of Eq1. The $\nu_s CH_2$ vibrations at 20 °C of Eq1, Eq2 and Hyd are 2850.3 cm^{-1}, 2850.8 cm^{-1} and 2849.4 cm^{-1}, respectively. It is the same tendency as observed with the CER NS/CHOL/DFFA(C24), that is the $\nu_s CH_2$ wavenumber of Hyd is lower than that of Eq1 and Eq2 in the CER NS/CHOL/DFFA(C16). Fig. 3(C) and (D) show the $\nu_s CH_2$ and $\nu_s CD_2$ spectra at 20 °C in all processes, P1, P3 and P5 in Fig. 1. No significant difference of the peak width is observed between the spectra.

3.2. Shift of OR–HEX and HEX–LIQ phase transition temperatures

Table 1 shows the phase transition temperatures and the temperature ranges of the phase transition of the partially perdeuterated and fully protonated samples during the Hyd. When DFFAs in CER NS/CHOL/DFFAs replaces DFFA(C24), the T_{OR-HEX} increases by about 2 °C and the TW_{OR-HEX} decreases by 1 °C. This tendency in perdeuterated FFA containing samples is similar to that in protonated samples. When focusing on the $T_{HEX-LIQ}$ and $TW_{HEX-LIQ}$ in the $\nu_s CH_2$ and $\nu_s CD_2$

Table 1
Phase transition temperature after hydration. The CH_2 and CD_2 stretching plots are fitted with N-linear functions to determine the phase transition temperature and the temperature width of phase transition (N = 5 for the $\nu_s CH_2$ vibration of CER NS/CHOL/DFFAs and CER NS/CHOL/DFFA(C24), N = 3 for the $\nu_s CH_2$ vibration of CER NS/CHOL/DFFA(C16) and the $\nu_s CD_2$ vibration of three compositions).

Sample composition	Vibration mode	Phase transition temperature [°C]				Temperature width of phase transition [°C]			
		T_{OR-HEX}	S.D.	$T_{HEX-LIQ}$	S.D.	TW_{OR-HEX}	S.D.	$TW_{HEX-LIQ}$	S.D.
Totally-protonated samples									
CER NS/CHOL/FFAs	$\nu_s CH_2$	26.8	0.7	63.5	5.2	8.6	1.2	12.5	4.7
CER NS/CHOL/FFA(C24)	$\nu_s CH_2$	30.2	0.3	64.1	0.7	5.8	0.6	7.3	2.1
CER NS/CHOL/FFA(C16)	$\nu_s CH_2$	–	–	58.6	0.5	–	–	10.7	3.5
Perdeuterated samples									
CER NS/CHOL/DFFAs	$\nu_s CH_2$	26.1	0.5	65.5	8.0	6.2	0.6	10.8	7.1
	$\nu_s CD_2$	–	–	61.1	1.7	–	–	8.6	1.8
CER NS/CHOL/DFFA(C24)	$\nu_s CH_2$	28.0	1.8	62.5	2.7	5.1	0.4	12.7	7.1
	$\nu_s CD_2$	–	–	61.3	1.9	–	–	3.6	1.9
CER NS/CHOL/DFFA(C16)	$\nu_s CH_2$	–	–	63.0	9.0	–	–	12.6	7.4
	$\nu_s CD_2$	–	–	49.2	5.2	–	–	24.9	6.4

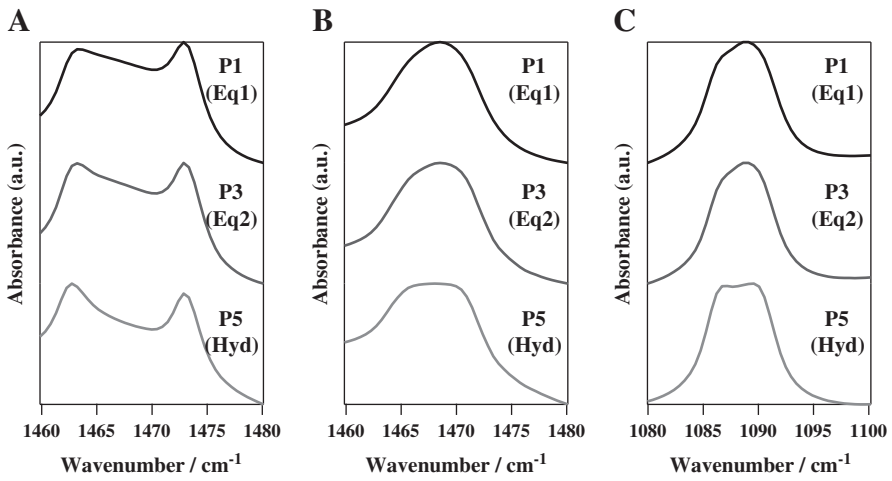

Fig. 4. Infrared spectra at 20 °C during Eq1, Eq2 and Hyd of the CER NS/CHOL/FFAs or CER NS/CHOL/DFFAs mixtures. The spectra of Eq1, Eq2 and Hyd of each sample correspond to the measurement points of P1, P3 and P5 in Fig. 1, respectively. (A) The spectra of the δCH_2 vibrations of the CER NS/CHOL/FFAs mixtures. (B) The spectra of the δCH_2 vibrations of the CER NS/CHOL/DFFAs mixtures. (C) The spectra of the δCD_2 vibrations of the CER NS/CHOL/DFFAs mixtures.

vibrations observed with the perdeuterated and fully protonated samples, no significant changes are observed, most probably also due to the larger standard deviations in the $T_{HEX-LIQ}$ and $TW_{HEX-LIQ}$ values. However, in the CER NS/CHOL/DFFA(C16), the $T_{HEX-LIQ}$ of the $\nu_s CD_2$ vibration is lower than that of the $\nu_s CH_2$ vibration, which is due to the individual phase change of the protonated and deuterated chains, see Fig. 2(D), (E) and (F). The $T_{HEX-LIQ}$ of the $\nu_s CH_2$ vibration in the CER NS/CHOL/FFA(C16) is about 58.6 °C, which may be induced by the individual phase change of the protonated chains of CER NS and FFA(C16).

3.3. Thermal behavior of the lateral packing of SC lipid models

Fig. 4(A) shows the δCH_2 spectra at 20 °C of the three heating runs of the equimolar CER NS/CHOL/FFA mixture at P1, P3 and P5, see Fig. 1. A slight splitting with peak positions at 1463.2 and 1473.0 cm^{-1} is already observed at P1 and P3. This demonstrates that a subpopulation of lipids forms an OR lattice. As the magnitude of the CH_2 splitting almost approaches the maximum value of 11 cm^{-1} large domains with an OR organization are formed [23]. However, as the dip between the peaks is not very steep, a substantial level of lipids is forming a HEX lateral packing. A clearer splitting, however, is observed at P5, that is after hydration. This suggests an increased level of lipids forming an OR phase. Upon heating, the spectra of three heating scans start to change to a broad peak at 28–30 °C (Eq1 and Eq2) and at 26–28 °C (Hyd). The vibrations turn into a singlet at 32–36 °C (Eq1 and Eq2) and at 30–34 °C (Hyd), indicating the formation of only a HEX phase.

In order to determine whether a change in fatty acid composition affects the mixing properties of CER NS and FFAs, the scissoring vibrations in the spectrum of the mixtures containing deuterated FFA were also examined. Fig. 4(B) and (C) show the δCH_2 and δCD_2 spectra at 20 °C at P1, P3 and P5, see Fig. 1. When focusing on the δCD_2 of the DFFA and the δCH_2 vibrations during Eq1 and Eq2, a single broad vibration is observed, which slightly increases in width after Hyd (P5). As no clear splitting is observed, no large phase separated OR domains of DFFAs exist in the mixture. Upon heating, the δCD_2 and δCH_2 spectra of Equilibration (Eq1 and Eq2) and Hyd turn into a singlet at 26–30 °C and 24–28 °C, respectively. This is in a similar temperature range as in the fully protonated mixtures, see Table 1. Our results suggest that the CER NS and DFFA participate in the same OR lattice in the equimolar CER NS/CHOL/DFFAs.

The δCH_2 and δCD_2 vibrations of the CERs/CHOL/FFA(C24) and CER NS/CHOL/DFFA(C24) mixtures are very similar to those described for the FFA and DFFA containing mixtures. However, the T_{OR-HEX} and $T_{HEX-LIQ}$ are slightly shifted to higher values. These results suggest that these lipid mixtures also form mixed crystals (data not shown).

The δCH_2 spectra of the CER NS/CHOL/FFA(C16) has also been examined. Fig. 5(A) shows the δCH_2 spectra at 20 °C at P1, P3 and P5 in Fig. 1. A slight splitting of the positions at 1465.5 and 1471.5 cm^{-1} is observed at P1. This demonstrates a coexistence of OR and HEX phases. Upon heating (Eq1), the spectra turn into a singlet at 38–46 °C, suggesting a phase transition to the HEX phase (data not shown). The δCH_2 spectrum at 20 °C (P3) of Eq2 shows a broad single peak at 1468 cm^{-1}, indicating the presence of mainly a HEX phase. The δCH_2 spectrum at 20 °C (P5) of the Hyd shows a weak splitting at 1464 and 1474 cm^{-1}, characteristic for the formation of domains with OR phase. However as the curve in between the two peaks is not very steep, a high level of the lipids are forming a HEX phase.

In order to examine whether the chain length matters for the mixing behavior the CER NS/CHOL/DFFA(C16) is also examined. Fig. 5(B) and (C) exhibit the δCH_2 and δCD_2 spectra at 20 °C at P1, P3 and P5 in Fig. 1. In the δCD_2 spectrum of the mixture at P1, three peaks are observed, a doublet located at 1086 and 1092 cm^{-1}, indicative for phase separation of the DFFA(C16) in an OR lattice and a weak singlet at 1089 cm^{-1}, suggesting that a fraction of DFFA(C16) and CER NS also mix. The δCH_2 and δCD_2 spectra at P3 show both a singlet peak at 1468 and 1089 cm^{-1}, respectively. As the FTIR spectrum of the CER NS/CHOL/FFA(C16) mixture also shows a HEX packing, but DFFA(C16) at 20 °C forms an orthorhombic lattice (see Discussion), our results suggest that DFFA(C16) is not phase separating in DFFA(C16) domains during the 2nd equilibration. However, interestingly, after hydration drastic changes are noticed. The spectra of the δCH_2 and δCD_2 vibrations exhibit quite broad vibration bands, the δCD_2 of which consists of three peaks (a slightly splitting peak and a weak single peak), respectively. These spectra of Hyd suggest that hydration enhances the phase separation between DFFA(C16) and CER in the mixture.

3.4. Direct visualization of lipid domains in SC lipid model

Fig. 6(A), (B) and (C) show Raman images, Map^D(CER NS), Map^D(CHOL) and Map^D(DFFAs) (the superscript D refers to the non-hydrated state of the lipid mixture), of the non-hydrated equimolar CER NS/CHOL/DFFA mixtures (RI1 in Fig. 1). The three maps show a rather homogeneous distribution, suggesting that the three lipid classes form a rather homogenous mixture, although some segregation occurs. Raman images were also monitored after hydration (RI2 in Fig. 1), which are shown in Fig. 6(D), (E) and (F). Several domains enriched in CHOL are observed in Map^H(CHOL), while several domains with a

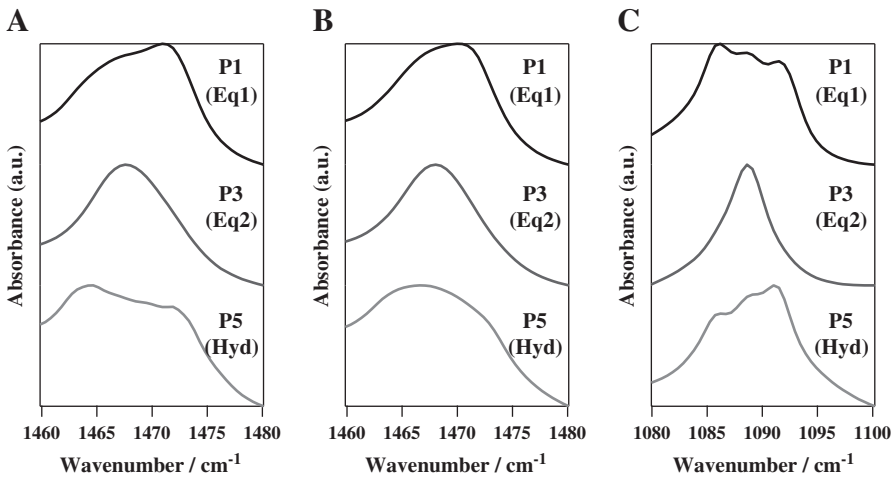

Fig. 5. Infrared spectra of the CER NS/CHOL/FFA(C16) and CER NS/CHOL/DFFA(C16) mixtures. The spectra of Eq1, Eq2 and Hyd of each sample correspond to the measurement points of P1, P3 and P5 in Fig. 1, respectively. (A) The spectra of the δCH_2 vibrations of the CER NS/CHOL/FFA(C16) mixtures. (B) The spectra of the δCH_2 vibrations of the CER NS/CHOL/DFFA(C16) mixtures. (C) The spectra of the δCD_2 vibrations of the CER NS/CHOL/DFFA(C16) mixtures.

decreased level in CER NS and DFFAs are observed in Map^H(CER NS) and Map^H(DFFAs), respectively (the superscript H refers to the hydrated state of the lipid mixture). Although the CHOL-rich domains correspond to the CER NS-poor and DFFAs-poor domains, the CER NS and DFFA show a rather homogeneous distribution. The reproducibility of results was confirmed by measuring at least two samples.

Fig. 7(A), (B) and (C) show the three maps of the non-hydrated equimolar CER NS/CHOL/DFFA(C16) mixture (RI1 in Fig. 1). Each map shows large regions enriched (lighter) or diminished (darker) in each of the lipid classes. However, the contrast between the lighter and darker regions is not so strong, indicating that the lipid mixture demonstrates a similar deviation in homogeneous distribution for all three components. After hydration, however (see Fig. 7(D), (E) and (F)), several domains enriched in CHOL are observed in the Map^H(CHOL), corresponding to several domains diminished in CER NS and DFFA(C16) observed in the Map^H(CER NS) and Map^H(DFFAs), respectively. The reproducibility of results was confirmed by measuring at least two samples.

3.5. Time-dependent change of lipid organization in SC lipid models

We also examined whether the mixing properties of hydrated mixtures change when exposed to higher temperature or storage. Fig. 8 shows the contours of the δCD_2 and δCH_2 vibrations in the hydrated CER NS/CHOL/DFFAs and CER NS/CHOL/DFFA(C16). Each figure includes 5 spectra, which show the spectra at P5, P6, P7, P8 and P9 (see schematic view in Fig. 1), corresponding to Hyd, After-Hyd, 1 month After-Hyd, 2 months After-Hyd and 3 months After-Hyd, respectively. Broad peaks in the δCD_2 and δCH_2 vibrations in all spectra of the CER NS/CHOL/DFFAs demonstrate that the lipid mixture do not phase separate, even during 3 months storage, see Fig. 8(A) and (B), except that the broad peaks of the δCD_2 and δCH_2 vibrations in the spectrum of the After-Hyd are somewhat sharper compared with that in the Hyd. When replacing DFFAs by DFFA(C24) the time-dependent change of the contours of the δCD_2 and δCH_2 vibrations in the CER NS/CHOL/DFFA(C24) remains very similar (data not shown).

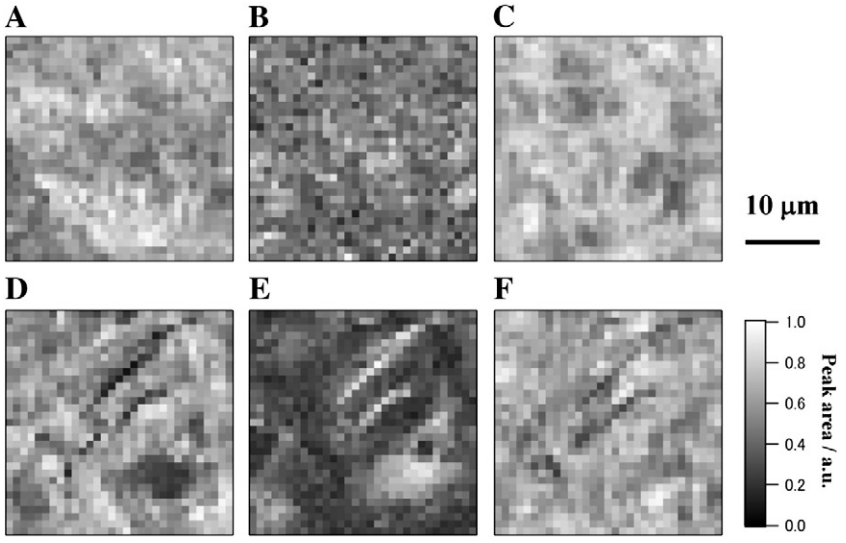

Fig. 6. Raman images corresponding to CER NS, CHOL and DFFAs for the CER NS/CHOL/DFFAs collected over an area 30 × 30 μm^2. 2nd equilibration process (A–C) and hydration process (D–F).

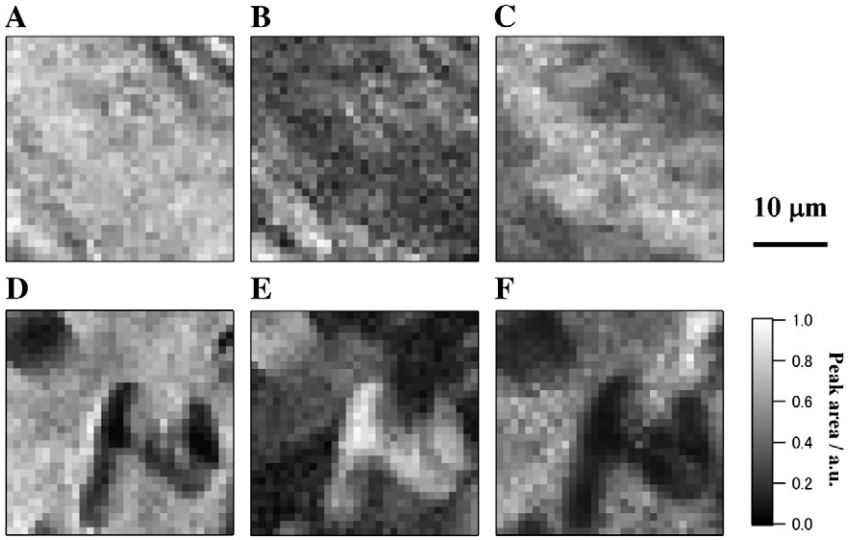

Fig. 7. Raman images corresponding to CER NS, CHOL and DFFA(C16) for the CER NS/CHOL/DFFA(C16) collected over an area 30 × 30 μm^2. 2nd equilibration process (A–C) and hydration process (D–F).

The spectrum of the CER NS/CHOL/DFFA(C16) mixture reveals broad peaks in the δCD_2 and δCH_2 vibrations of the After-Hyd, see Fig. 8(C) and (D). As at 20 °C pure DFFA(C16) forms an OR lattice (see Fig. 9) the presence of a singlet indicates that DFFA does not phase separate due to the heating and equilibration at elevated temperature. After storage for 1 month, however, three clear peaks are observed of the δCD_2 vibrations, while a broad peak is observed of the δCH_2 vibrations. The spectra of 2 and 3 months After-Hyd are similar to that of 1 month After-Hyd. This demonstrates that the DFFA(C16) phase separates, while a small fraction of CER NS induces the formation of an OR lateral packing.

4. Discussion

To understand the lipid phase behavior in the SC in detail, model lipid mixtures have been examined varying from one component systems to multicomponent systems. However, until now no direct comparison has been made between simplified mixtures and complex mixtures on the lipid phase behavior. In this study, we focused on the effect of i) the complexity of the FFA mixture and ii) the mismatch of hydrocarbon chains between CER and FFA on their mixing properties. In addition we studied the effect of i) heating and cooling, ii) hydration and iii) storage on the lipid phase behavior.

4.1. Equilibration induces highly ordered alkyl chains of CER which forms the mixed crystal

The ordering of the hydrocarbon chains are measured by frequencies of the $\nu_s CH_2$ and $\nu_s CD_2$ vibrations. These are conformation-sensitive, that is depending on the ratio of the *trans-gauche* conformations in the alkyl chains [15,27]. In this study three heating and cooling processes were performed and Eq1 and Eq2 were measured with the lipid mixtures in a dry state, while the 3rd heating/cooling process (Hyd) was with the lipid mixture in a hydrated state. During Eq1 and subsequent cooling of CER NS/CHOL/DFFAs and CER NS/CHOL/DFFA(C24) the $\nu_s CH_2$ vibrations at 20 °C changed compared to prior heating: a decrease in peak width and a small shift in wavenumber to lower values are observed. The obtained $\nu_s CH_2$ contours show that after Eq1 and cooling the acyl chains of CER NS are already a tightly packed fully extended highly ordered all-*trans* conformation. No significant difference in the $\nu_s CD_2$ vibrations at 20 °C is observed before and after Eq1. This may be due to a decreased sensitivity of the $\nu_s CD_2$ vibrations to small changes in the conformation of the deuterated chain, which is also demonstrated by the absence of the OR–HEX transition in the thermotropic $\nu_s CD_2$ spectra. In contrast, no significant difference in the peak width of the $\nu_s CH_2$ vibrations in all processes is observed in the CER NS/CHOL/DFFA(C16). The peak width is narrow and the peak position is below 1089 cm^{-1}, suggesting that CER NS exists in the all-*trans* conformation.

4.2. The mismatch between FFAs and the acyl chain of CER NS is a determinant factor for phase separation

When comparing the mixing properties of the CER NS/CHOL/DFFA(C24) and CER NS/CHOL/DFFA(C16), clear differences are observed. The spectra of CER NS/CHOL/DFFA(C24) show single δCH_2 and δCD_2 vibrations during the sample equilibration and hydration procedure. As δCH_2 of the CER NS/CHOL/FFA(C24) mixtures show a splitting in the contours, this indicates that CER NS/CHOL/DFFA(C24) form mixed crystals, in which a subpopulation of lipids forms an orthorhombic lateral packing. The spectra of the CER NS/CHOL/DFFA(C16) mixture at 20 °C during Eq1 and Hyd exhibit a tendency of phase separation. As pure DFFA(C16) shows a clear splitting at 20 °C, demonstrating the presence of an OR phase, see Fig. 9, the splitting in δCD_2 vibration in the spectra of the CER NS/CHOL/DFFA(C16) mixture is due to phase separated DFFA(C16). This indicates that the slight splitting of the δCH_2 contour in the protonated CER NS/CHOL/DFFA(C16) during Eq1 and Hyd is likely due to domains of phase separated FFA(C16) surrounded by lipids forming a hexagonal lateral packing. The differences between the FFA(C24) and FFA(C16) containing mixtures strongly suggests that a mismatch of chain length of the acyl chain of CER NS and the FFA chain is a determinant factor for phase separation. This is of interest as the sphingoid base chain being C18 in chain length and thus matching more closely the chain length with DFFA(C16) than with DFFA(C24) seems to play a less prominent role in the mixing properties. Furthermore, very recently we also observed that in the SC lipid membrane CHOL can compensate for FFA(C24), the acyl chain of which straddles the unit cell center [28]. This may also enhance the mixing properties within the lipid layer. In a previous paper, it has also been reported that the phase behavior, the lipid mixing properties and the transition temperatures strongly depend on the FFA chain length in ternary model lipid mixtures. However, in those studies CER from bovine brain were used having a chain length distribution of acyl chain [26].

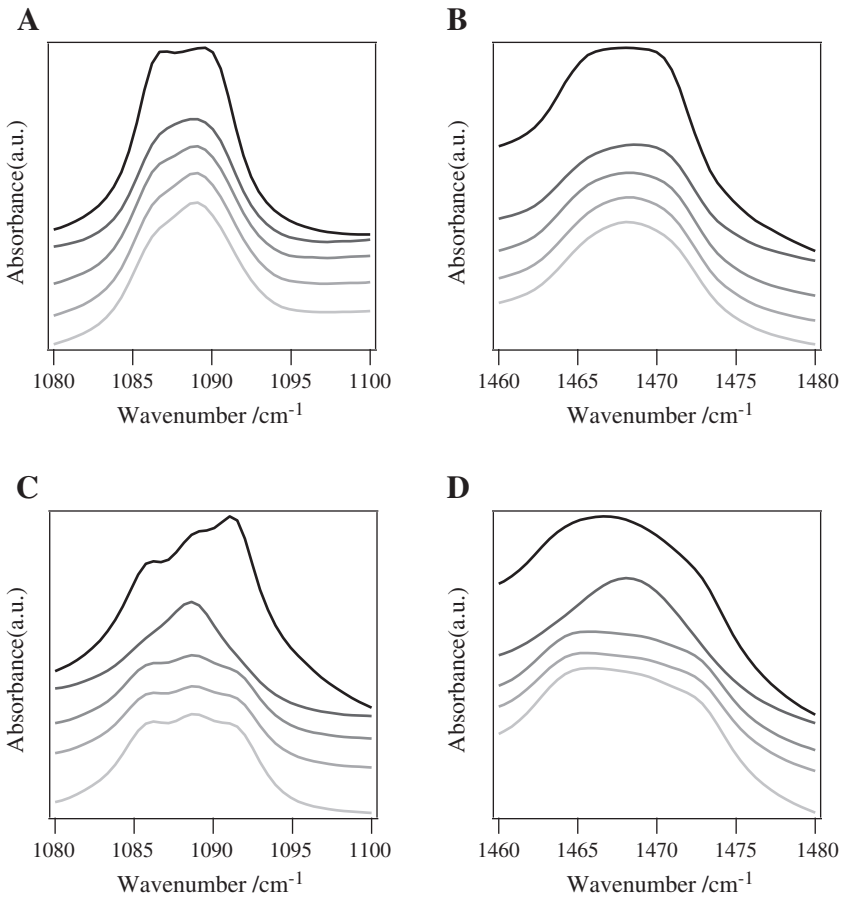

Fig. 8. Time-dependent change of the contours of the δCD_2 and δCH_2 δ °C. From top to the bottom Hyd (P5), After-Hyd (P6), 1 month after (P7), 2 months after (P8) and 3 months after (P9). (A) The spectra of the δCD_2 vibrations of the CER NS/CHOL/DFFAs. (B) The spectra of the δCH_2 vibrations of the CER NS/CHOL/DFFAs. (C) The spectra of the δCD_2 vibrations of the CER NS/CHOL/DFFA(C16). (B) The spectra of the δCH_2 vibrations of the CER NS/CHOL/DFFA(C16).

When extrapolating our results to the lipids in the human SC, always a wide variation in chain length is observed. Therefore, a pahse separation between CERs and FFAs is not expected to occur. However, when in diseased skin a high level of short chain FFAs is present in the SC [29], our data suggest that there is an increased chance for phase separation between CERs and FFAs.

4.3. Hydration is a driving force for phase separation

When comparing the δCH_2 vibration in the spectrum of CER NS/CHOL/FFA(C16) and CER NS/CHOL/FFA(C24) before and after hydration, also clear differences are observed: hydration induces a broadening of the δCH_2 and δCD_2 vibrations of the CER NS/CHOL/DFFAs and CER NS/CHOL/DFFA(C24) and a splitting of these vibrations in the spectra of the CER NS/CHOL/DFFA(C16) mixtures. This suggests that in mixtures prepared with CER NS hydration induces phase separation, but the degree of phase separation depends on the FFA chain length. The phase separation induced by hydration is also observed in the Raman images: while a rather homogeneous distribution of three components, CER NS, CHOL and DFFA(C16) is observed before hydration, domains of each of the components are more prominently present after hydration.

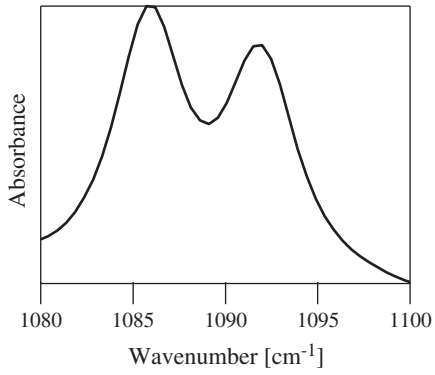

Fig. 9. FTIR spectrum of the δCD_2 vibrations of the DFFA(C16) collected at 20 °C in Eq2.

There is also an interesting observation when focusing on the phase behavior during storage of the CER NS/CHOL/DFFA(C16) mixture. While after hydration the DFFA(C16) phase separates to some extent, subsequent heating and cooling of the mixture enhances the degree of mixing of CER NS and FFA(C16). However, this mixing is only temporary as during the successive storage phase separation is observed already after 1 month storage. It seems that in a hydrated state the equilibrium situation in this mixture is a moderate phase separation between FFA(C16) and CER NS.

4.4. Hydration of lipid mixtures causes a reduction in transition temperature of the OR–HEX transition

The lipid mixtures of the CER NS/CHOL/FFAs and CER NS/CHOL/FFA(C24) form mixed OR crystals. After hydration the mid-temperature of the OR–HEX phase transition decreases 2–3 °C. Previous studies also have reported that the hydration of human SC reduces the phase

transition temperature of the intercellular lipids to decrease by 5–8 °C [30–32]. Therefore our data show a similar trend to that observed in the SC. This decrease in phase transition temperature was also observed for the CER NS/CHOL/FFA(C16). We speculate that this shift in transition temperature may be due to a weakening of hydrogen bonds between the opposing head groups of the lipid bilayers due to incorporation of a small amount of water into the neighboring layers of head groups. There is indeed evidence for the presence of low levels of water between the head group regions: i) X-ray diffraction studies indicated a slight swelling of the short periodicity lamellar phase in human SC and hairless mouse SC [33,34] and ii) it is reported that in lipid model systems around 2 molecules of water are present per lipid molecule [35].

4.5. The chain length distribution of FFA affects the phase transition temperature of the lipid mixture

In this study, the presence FFA(C24) increases the T_{OR-HEX} and decreases TW_{OR-HEX} compared to the lipid mixture containing the FFAs with wide variations in chain lengths. In a previous study, the influence of the FFA chain length in the thermal phase behavior of SC lipid models has been investigated and showed that FFA with a shorter chain length results in a lower T_{OR-HEX} phase transition [26]. Therefore most likely, the presence of shorter fatty acids in the FFA mixture is responsible for the reduction in the T_{OR-HEX} phase transition temperature of the mixed crystal.

4.6. Mixing after spraying and phase separation after hydration are stable, while mixing after heating may be not an equilibrium situation

Unexpectedly, the broad peaks of the δCH_2 and δCD_2 vibrations at 20 °C of Eq1 (Fig. 1, P1) in the CER NS/CHOL/DFFAs and CER NS/CHOL/DFFA(C24) indicate that these lipid mixtures form a mixed crystal phase even after spraying the lipids on the AgBr crystal without any heating–cooling process. These mixtures do not show significant changes in FTIR spectrum during subsequent equilibration and hydration steps. In contrast to this, the phase separation in the CER NS/CHOL/DFFA(C16) mixture is sensitive to the history of the sample. This suggests that the matching of the chain lengths of FFA and acyl chains of the CER NS might be an important factor for the stability of the ternary SC lipid models. Several papers have investigated the kinetics of lipid mixtures by FTIR [14,17,36–37]. SC lipid models prepared from CER/CHOL/DFFA(C18) (this CER is a CER NS or CER AS with an acyl chain length of either C18:0, C24:0 and C24:1) showed the presence of phase separated domains in time, even though a mixed crystal was formed just after rapidly cooling, similarly as we noticed in our studies after hydration of the CER NS/CHOL/DFFA(C16) mixture [36]. These reported time-dependent changes depended on hydration, lipid composition and thermal history of the sample.

5. Conclusions

The present study shows the thermotropic phase behavior and mixing properties of CER NS/CHOL/FFA mixtures during preparation and storage of the ternary SC lipid mixtures. The heating/cooling curves, the hydration of lipid mixtures and the storage induce changes in the mixing properties that were highly dependent on the composition of the FFAs. While in a complex mixture of FFA and a single FFA(C24) only minor and similar effects were observed, in mixtures containing FFA(C16) phase separation was observed after hydration and long term storage. As the acyl chain of CER NS is C24, it seems that matching of the chain length of FFA and acyl chain of CER promotes the mixing. Our studies demonstrate that the thermotropic phase behavior and the mixing properties of lipid mixtures strongly depend on the chain length and the hydration state of the lipid mixtures.

References

[1] A.S. Michaels, S.K. Chandrasekaran, J.E. Shaw, Drug permeation through human skin: theory and in vitro experimental measurement, AIChE J 21 (1975) 985–996.
[2] O. Simonetti, A.J. Hoogstraate, W. Bjalik, J.A. Kempenaar, A.H.G.J. Schrijvers, H.E. Boddé, M. Ponec, Visualization of diffusion pathways across the stratum corneum of native and in-vitro-reconstructed epidermis by confocal laser scanning microscopy, Arch. Dermatol. Res. 287 (1995) 465–473.
[3] P.W. Wertz, M.C. Miethke, S.A. Long, J.H. Strauss, D.T. Downing, Composition of the ceramides from human stratum corneum and from comedones, J. Invest. Dermatol. 84 (1985) 410–412.
[4] K.J. Robson, M.E. Stewart, S. Michelsen, N.D. Lazo, D.T. Downing, 6-Hydroxy-4-sphingenine in human epidermal ceramides, J. Lipid Res. 35 (1999) 2060–2068.
[5] J.A. Bouwstra, G.S. Gooris, J.A. van der Spek, W. Bras, Structural investigations of human stratum corneum by small-angle X-ray scattering, J. Invest. Dermatol. 97 (1991) 1005–1012.
[6] S.H. White, D. Mirejovsky, G.I. King, Structure of lamellar lipid domains and corneocyte envelopes of murine stratum corneum. An X-ray diffraction study, Biochemistry 27 (1988) 3725–3732.
[7] J.A. Bouwstra, G.S. Gooris, M. Ponec, The lipid organisation of the skin barrier: liquid and crystalline domains coexist in lamellar phases, J. Biol. Phys. 28 (2002) 211–223.
[8] I. Hatta, N. Ohta, K. Inoue, N. Yagi, Coexistence of two domains in intercellular lipid matrix of stratum corneum, Biochim. Biophys. Acta 1758 (2006) 1830–1836.
[9] L. Norlén, I. Nicander, A. Lunsjö, T. Cronholm, B. Forslind, A new HPLC-based method for the quantitative analysis of inner stratum corneum lipids with special reference to the free fatty acid fraction, Arch. Dermatol. Res. 290 (1998) 508–516.
[10] J. van Smeden, L. Hoppel, R. van der Heijden, T. Hankemeier, R.J. Vreeken, J.A. Bouwstra, LC/MS analysis of stratum corneum lipids: ceramide profiling and discovery, J. Lipid Res. 52 (2011) 1211–1221.
[11] N. Ohta, I. Hatta, Interaction among molecules in mixtures of ceramide/stearic acid, ceramide/cholesterol and ceramide/stearic acid/cholesterol, Chem. Phys. Lipids 115 (2002) 93–105.
[12] M.E. Rerek, D.V. Wyck, R. Mendelsohn, D.J. Moore, FTIR spectroscopic studies of lipid dynamics in phytosphingosine ceramide models of the stratum corneum lipid matrix, Chem. Phys. Lipids 134 (2005) 51–58.
[13] G.S. Gooris, J.A. Bouwstra, Infrared spectroscopic study of stratum corneum model membranes prepared from human ceramides, cholesterol, and fatty acids, Biophys. J. 92 (2007) 2785–2795.
[14] M. Lafleur, Phase behaviour of model stratum corneum lipid mixtures: an infrared spectroscopy investigation, Can. J. Chem. 76 (1998) 1501–1511.
[15] D.J. Moore, M. Rerek, Role of ceramides 2 and 5 in the structure of the stratum corneum lipid barrier, Int. J. Cosmet. Sci. 21 (1999) 353–368.
[16] V. Velkova, M. Lafleur, Influence of the lipid composition on the organization of skin lipid model mixtures: an infrared spectroscopy investigation, Chem. Phys. Lipids 117 (2002) 63–74.
[17] P. Garidel, B. Fölting, I. Schaller, A. Kerth, The microstructure of the stratum corneum lipid barrier: mid-infrared spectroscopic studies hydrated ceramide: palmitic acid: cholesterol model systems, Biophys. Chem. 150 (2010) 144–156.
[18] D. Groen, D.S. Poole, G.S. Gooris, J.A. Bouwstra, Investigating the barrier function of skin lipid models with varying compositions, Eur. J. Pharm. Biopharm. 79 (2011) 334–342.
[19] S. Motta, M. Monti, S. Sesana, R. Caputo, S. Carelli, R. Ghidoni, Ceramide composition of the psoriatic scale, Biochim. Biophys. Acta 1182 (1993) 147–151.
[20] P. Wertz, Epidermal lipids, in: L.A. Goldsmith (Ed.), Physiology, Biochemistry and Molecular Biology of the Skin, Oxford University Press, Oxford, 1991, pp. 205–235.
[21] R.G. Snyder, G.L. Strauss, C. Ellinger, C – H stretching modes and the structure of *n*-alkyl chains. 1 long, disordered chains, J. Phys. Chem. 86 (1982) 5145–5150.
[22] R.G. Snyder, G.L. Liang, H.L. Strauss, R. Mendelsohn, IR spectroscopic study of the structure and phase behaviour of long-chain diacylphosphatidylcholines in gel-phase, J. Biophys. 71 (1996) 3186–3198.
[23] R. Mendelsohn, G.L. Liang, H.L. Strauss, R.G. Snyder, IR spectroscopic determination of gel state miscibility in long-chain phospatidylcholine mixtures, Biophys. J. 69 (1995) 1987–1998.
[24] V.R. Kodati, R. El-Jastimi, M. Lafleur, Contribution of the intermolecular coupling and librotorsional mobility in the methylene stretching modes in the infrared spectra of acyl chains, J. Phys. Chem. 88 (1994) 12191–12197.
[25] M.W. de Jager, G.S. Gooris, M. Ponec, J.A. Bouwstra, Lipid mixtures prepared with well-defined synthetic ceramides closely mimic the unique stratum corneum lipid phase behavior, J. Lipid Res. 46 (2005) 2649–2656.
[26] X. Chen, S. Kwak, M. Lafleur, M. Bloom, N. Kitson, J. Thewalt, Fatty acids influence "solid" phase formation in models of stratum corneum intercellular membranes, Langmuir 23 (2007) 5548–5556.
[27] H.L. Casal, H.H. Mantsch, Polymorphic phase behaviour of phospholipid membranes studied by infrared spectroscopy, Biochim. Biophys. Acta 779 (1984) 381–401.
[28] E.H. Mojumdar, D. Groen, G.S. Gooris, D.J. Barlow, M.J. Lawrence, B. Deme, J.A. Bouwstra, Localization of cholesterol and fatty acid in a model lipid membrane: a neutron diffraction approach, Biophys. J. 105 (2013) 911–918.
[29] J. van Smeden, M. Janssens, E.C.J. Kaye, P.J. Caspers, A.P. Lavrijsen, R.J. Vreeken, J.A. Bouwstra, The importance of free fatty acid chain length for the skin barrier function in atopic eczema patients, Exp. Dermatol. 23 (2014) 45–52.

[30] G.M. Golden, D.B. Guzek, R.R. Harris, J.E. McKie, R.O. Potts, Lipid thermotropic transitions in human stratum corneum, J. Invest. Dermatol. 86 (1986) 255–259.
[31] C.L. Gay, R.H. Guy, G.M. Golden, V.H.W. Mak, M.L. Francoeur, Characterization of low-temperature (i.e., <65 °C) lipid transitions in human stratum corneum, J. Invest. Dermatol. 103 (1994) 233–239.
[32] J. Caussin, G.S. Gooris, M. Janssens, J.A. Bouwstra, Lipid organization in human and porcine stratum corneum differs widely, while lipid mixtures with porcine ceramides model human stratum corneum lipid organization very closely, Biochim. Biophys. Acta 1778 (2008) 1472–1482.
[33] H. Nakazawa, N. Ohta, I. Hatta, A possible regulation mechanism of water content in human stratum corneum via intercellular lipid matrix, Chem. Phys. Lipids 165 (2012) 238–243.
[34] N. Ohta, S. Ban, H. Tanaka, S. Nakata, I. Hatta, Swelling of intercellular lipid lamellar structure with short repeat distance in hairless mouse stratum corneum as studied by X-ray diffraction, Chem. Phys. Lipids 123 (2003) 1–8.
[35] D. Groen, G.S. Gooris, D.J. Barlow, M.J. Lawrence, J.B. van Mechelen, B. Demé, J.A. Bouwstra, Disposition of ceramide in model lipid membranes determined by neutron diffraction, Biophys. J. 100 (2011) 1481–1489.
[36] D.J. Moore, R.G. Snyder, M.E. Rerek, R. Mendelsohn, Kinetics of membrane raft formation: fatty acid domains in stratum corneum lipid, J. Phys. Chem. B 110 (2006) 2378–2386.
[37] M. Gorcea, J. Hadgraft, D.J. Moore, M.E. Lane, Fourier transform infrared spectroscopy studies of lipid domain formation in normal and ceramide deficient stratum corneum lipid models, Int. J. Pharm. 435 (2011) 63–68.